DEUTSCHES ELEKTRONEN-SYNCHROTRON DESY

DESY SR 84-36
December 1984

DYNAMICAL DIFFRACTION OF X-RAY SPHERICAL WAVES IN PERFECT CRYSTALS USING A NARROW SLIT AS RADIATION SOURCE

by

V.V. Aristov, V.I. Polovinkina, A.A. Snigirev

Inst. of Problems of Microelectronics Technology & Superpure Materials, Academy of Sciences of the USSR, Chernogolovka

W. Graeff

Hamburger Synchrotronstrahlungslabor HASYLAB at DESY

Eigentum der Property of DESY Bibliothek library
Zugang: Accessions: 11. FEB. 1985
Leihfrist: Loan period: 7 Tage days

ISSN 0723-7979

NOTKESTRASSE 85 · 2 HAMBURG 52

DESY behält sich alle Rechte für den Fall der Schutzrechtserteilung und für die wirtschaftliche Verwertung der in diesem Bericht enthaltenen Informationen vor.

DESY reserves all rights for commercial use of information included in this report, especially in case of filing application for or grant of patents.

To be sure that your preprints are promptly included in the
HIGH ENERGY PHYSICS INDEX ,
send them to the following address (if possible by air mail) :

DESY
Bibliothek
Notkestrasse 85
2 Hamburg 52
Germany

DESY SR 84-36
December 1984

ISSN 0723-7979

DYNAMICAL DIFFRACTION OF X-RAY SPHERICAL WAVES IN PERFECT CRYSTALS USING A NARROW SLIT AS RADIATION SOURCE

V.V. Aristov (a)
W. Graeff (b)
V.I. Polovinkina (a)
A.A. Snigirev (a)

(a) Institute of Problems of Microelectronics Technology
and Superpure Materials, Academy of Sciences of the USSR
Chernogolovka 142432 Moscow district, USSR.

(b) Hamburger Synchrotronstrahlungslabor HASYLAB
at
Deutsches Elektronensynchrotron DESY
2000 Hamburg 52, Germany.

submitted to phys. stat. sol.

ABSTRACT

Dynamical diffraction of X-ray spherical waves in perfect crystals has been realized experimentally using white synchrotron radiation collimated by a narrow slit. In the Laue case the diffraction of a narrow collimated beam in a wedge shaped crystal looks like that of the X-ray spherical wave diffraction. It exhibits such phenomena like focusing of the weakly absorbed wavefield, ordinary and anomalous Pendellösung fringes. The interference patterns of wavefields in the beams of a two-crystal interferometer have also been obtained at different slit-to-film distances.

Classification:

1.1

1. INTRODUCTION

The diffraction pattern of a X-ray spherical wave diffracted by a perfect crystal is determined by the phase change of this wave in the crystal and in vacuum on its way from the source to the film [1,2]. In other words the look of the pattern depends on the parameter t/L, where t is the crystal thickness and L is the source to film distance. So far all our experimental studies of the effect of the parameter t/L on the diffraction pattern have been carried out using a point source of radiation. But in traditional X-ray topography when taking section patterns a narrow slit is used which is interpreted as a point source. It has been shown theoretically [3,4] that a narrow slit with a width smaller than the extinction length can be considered as an incoherent source of spherical (strictly speaking cylindrical) waves all the parameters of the diffraction pattern being dictated by the distance from the slit rather than from the real source. This is particularly evident in the case of section topography with synchrotron radiation where usually the source is 20 - 80 m away from the sample.

In the present paper the X-ray spherical wave diffraction in a wedge shaped crystal as well as in a two-crystal interferometer has been studied experimentally using a narrow slit as the radiation source to observe the effects of dynamical diffraction with allowance for additional interference phenomena in vacuum (focusing, anomalous Pendellösung fringes etc.).

2. EXPERIMENTS.

The study was performed at the HASYLAB topography station using synchrotron radiation from the storage ring DORIS. The experimental set-up is schematically shown in Fig.1. The source distance of the topography station is L_0 = 34 m. The beam cross section was precollimated to 0.1 x 6 mm^2 and finally collimated by a slit formed of two parallel steel cylinders with 3 mm diameter and a gap of 1 mm between them. By turning the slit with respect to the beam a visible gap (i.e. the slit width) was adjusted to 1 - 5 μm. When placing the slit in the orbital plane of the storage ring about 80 - 90 percent of the radiation is linearly polarized so that a vertical diffraction plane was chosen to observe the diffraction of the σ-polarized radiation.

Specimens were cut from dislocation-free Si single crystals grown by Czochralski's technique. The growth axis was [111]. The wedge shaped specimen and the two-crystal interferometer were polished mechanically and chemically.

The diffraction images of the crystals were taken without any premonochromatization at the wavelengths λ = 1 A and 1.2 A which lie close to the critical wavelength of the radiation spectrum. This choice of wavelength enabled us to eliminate the contribution of higher harmonics λ/n to the (111) and (220) images[1] . The images were recorded on a fine grain X-ray film (Kodak Industrex type R) with an exposure time ranging from 20 to 150 s.

3. RESULTS AND DISCUSSION.

3.1 Dynamical diffraction in a perfect crystal

The topograph from the wedge shaped Si crystal was obtained in the symmetrical (111) Laue case reflection. With a Bragg angle Θ_B = 11.5° the Bragg condition for this reflection is fulfilled with λ = 1.2 A. To meet the geometrical focusing condition of the image [6] with this wavelength the slit-to-specimen and the specimen-to-film distances were $L_1 = L_2$ = 0.38 m.

In the topograph shown in Fig. 2 one can easily see the details which are characteristic of the X-ray spherical wave diffraction in a wedge shaped crystal when the image structure is significantly influenced by the additional phase changes of the interfering waves along their vacuum path.

At a crystal thickness t = 50 - 70 μm the weakly absorbed wavefield is focused [1,2]; at t < 50 μm the image of the wedge tip shows anomalous Pendellösung fringes [2]; at t > 70 μm the interference pattern is observed as alternating dark and light spots that gradually turn to the ordinary Pendellösung fringes with increasing thickness [2,7].

---

[1] In the topographs first obtained at λ = 2 A for the (111) - reflection we have observed a superposition of two orders of reflection (along with the authors of work [5]), the intensity of the (333) reflection being considerably larger than that of the (111) reflection due to the large difference in the absorption of λ = 2 A and $\lambda/3 \sim 0.7$ A.

Let us compare the experimentally observed thickness of focusing with the theoretical one, t_s, which is equal to

$$t_s = \lambda(L_1+L_2)/(2\Lambda\sin^2\Theta_B) \qquad (1)$$

where Λ is the extinction length. In our case for σ-polarized radiation we have $\Lambda = 23$ μm. With $L = L_1 + L_2 = 0.76$ m, $\lambda = 1.2$ A and $\Theta_B = 11.5°$ we obtain the focusing thickness $t_s = 50$ μm. The calculated value of t_s is, as usual [2,8], underestimated compared to the experimental one. This is connected with the fact that the strongest focusing occurs at a thickness somewhat larger than t_s [2] where the radiation is focused out of two overlapping angular regions that correspond to two points on the dispersion surface.

Thus the observed diffraction pattern corresponds to the theoretical one without any extra details which confirms the assumption that the slit acts like an incoherent source of spherical waves.

Having a slit width of the order of several microns the diffraction at the slit gives an angular divergence of the central diffraction peak $\Delta\Theta \sim 10^{-5} - 10^{-4}$ rad which suffices to observe spherical wave interference effects [8]. The divergence resulting from the finite width of the synchrotron source is of the same order, namely $5\cdot10^{-5}$. This means that the condition for polychromatic focusing which must be distinguished from diffraction focusing has not to be fulfilled so stringently as in an experiment with a real point source at the slit position. A deviation $\Delta L = 10$ cm from the exact focusing distance would deteriorate the spatial resolution in the topograph by about 5 μm which is just at the resolution limit of the photoemulsion. Using a real point source such a deviation from the strict focusing condition would result in a 10 - 100 times larger blurring of the image.

Thus the use of synchrotron radiation collimated by a narrow slit makes it possible to vary the slit-to-film distance within several centimeters practically without any deterioration of the resolution. It should be noted again that this result was obtained without any premonochromatization of the radition.

3.2 Diffraction in the two-crystal interferometer

In the successive diffraction in two crystals the focusing of spherical waves can only take place at $L = 0$ provided the crystals are equally thick [9-11]. From the theory developed in [12] it follows that at $L \neq 0$ there exist three different thickness combinations for focusing. The diffraction pattern

including the focusing in the twice reflected beam that arises from successive diffraction in two different crystals and at $L \neq 0$ have already been observed experimentally [12]. The same experiments in a two-crystal interferometer have not been carried out because the polychromatic focusing in the twice reflected beam is impossible. In the light of the results presented in Section 3.1 it is of interest to study the effect of the parameter t/L on the diffraction pattern of a two-crystal interferometer.

The two-crystal interferometer consisted of a wedge shaped Si crystal and a plane parallel one 260 μm thick connected as usual by a common crystal base. The gap between the blocks was 10 mm. The splitting of the beams in the interferometer is schematically shown in Fig. 3. For beams E_{h0} and E_{0h} the polychromatic focusing is realized under the condition $L_1 = L_2$, while for E_{00} and E_{hh} this is impossible at all, hence the beam E_{hh} was observed at short distances only: $L_1 = L_2 = 10$ cm.

The detailed analysis made in [12] for the case of a twice diffracted beam enables a qualitative interpretation of the topographs of the beams E_{hh}, E_{h0} and E_{0h}.

When the source-to-film distance is finite, the diffraction pattern is substantially influenced by the parameter t_s and the angular variable q [12]

$$q = \pm\,[(t/t_s)^{2/3} - 1\,]^{1/2} \qquad (2)$$

where $t = t_1 + z_{ij}t_2$, t_1 and t_2 the thicknesses of the first and second crystal, respectively, and $z_{ij} = 1$ for $i = j$, $z_{ij} = -1$ for $i \neq j$.

The strongest focusing is observed in the center of the diffraction pattern of the beam E_{hh} corresponding to $q \sim 0$. In this case three combinations of crystal thicknesses are possible:

(1) $t_1 + t_2 = t_s$ the focusing of the BB - field[2]

Here the two crystals act as one crystal of summed thickness.

(2) $t_1 = t_2 + t_s$ the focusing of the BA - field

(3) $t_1 = t_2 - t_s$ the focusing of the AB - field

---

[2] Here and below the first (second) letter in the wavefield notation stands for the branch of the dispersion surface in the first (second) crystal. A denotes the highly absorbed wavefield and B the weakly absorbed one.

In our case type (1) focusing can only be observed when $t_s > t_2 = 260$ μm corresponding to L > 8.6 m which is practically not feasible due to the lack of polychromatic focusing. In cases (2) and (3) those wavefields are focused that belong in different crystals to different branches of the dispersion surface. These cases are also realized in the limit $t_s = 0$ (L = 0) under the condition of a "thin" crystal, $\mu t < 1$, where μ is the linear absorption coefficient, which means $t_1 = t_2$ [9-11]. The two focused wavefields superpose and their interference yields the high sensitivity of the topograph in the focused region to deformations and changes in crystal orientation [11].

The geometry of the interference pattern produced by spherical wave diffraction in two crystals is schematically presented in Fig. 4. In the first crystal there exist two wavefields corresponding to the two branches of the dispersion surface: A is the divergent and B is the convergent field. Both fields excite in the second crystal four wavefields: AA, AB, BB and BA. The caustics of the AB- field are directed to the region of smaller thickness and those of the BA- field to the region of larger thickness. These caustics divide the interference pattern into four regions, each representing the interference of specific wavefield combinations [12]:

I AB + BB

II, III AA + BB

IV BA + BB

Experimental topographs of beams E_{hh}, E_{h0} and E_{0h} are shown in Fig. 5 for $L_1 = L_2 = 0.1$ m. The central regions I and IV are clearly seen in the image of E_{hh} (Fig. 5a) as interference fringes, restricted by two pairs of caustics converging to the center. From the above considerations we expect focusing at two different thicknesses of the first wedge shaped crystal: $t_1 =$ 254 μm and 266 μm due to a separate focusing of the AB- and BA- fields at L ≠ 0 (corresponding to $t_s = 6$ μm).

The boundaries of the visible image of the beam E_{h0} (Fig. 5b) are determined mainly by the Borrmann fan of the first wedge shaped crystal. Therefore the topograph shows a wedge shaped image consisting of regions III and IV. Region I manifests itself only at the very end of the wedge.

The beam E_{0h} (Fig. 5c) is formed by the Borrmann fan of the second plane parallel crystal and consists basically of regions I and II. Only the thick part of the wedge images interference fringes corresponding to region IV.

With increasing distance L (L = 80 cm, $L_1 = L_2 = 40$ cm) the foci of the AB- and BA- fields undergo considerable splitting : $\Delta t = 2\ t_s \sim 50$ μm. This makes the interference pattern more complicated (Fig. 6).

In the region of small thickness caustics of the virtual focus of the BB-field appear (compare with the diagram in Fig.4) and the image of the E_{h0}-beam becomes sharper (Fig. 6a). The anomalous Pendellösung effect due to the interference of BA- and AA- waves is also present in this region ($t_1 \to 0$). The region between the split foci also undergoes considerable changes : extra interference of wavefields are clearly seen in the topographs (enlarged portion of Fig. 6).

As the distance L is increased the interference contrast is getting worse whereas the spatial resolution is insignificantly deteriorated when changing L from 20 to 80 cm. It is possible that the deterioration of the contrast is connected with the complication of the interference pattern due to the superposition of different interfering waves.

4. CONCLUSION

The experimental results have shown that a narrow slit placed in front of a crystal acts as an incoherent source of radiation when producing section topographs. All features of the interference pattern in the topograph are conditioned by the focal size of the source and the slit-to-film distance. The experiments on the diffraction focusing in a single crystal as well as in a two-crystal interferometer have been carried out for the first time using synchrotron radiation. It should be noted that the experimental setup for producing topographs with the use of focusing is simpler and of higher luminous power than those used earlier [2,8] and enabled us to produce for the first time topographs of a two-crystal interferometer at L ≠ 0. Our investigations show the possibility to construct experimental setups aimed at the study of defect contrasts in section topographs produced under various conditions of dynamical focusing of wavefields.

REFERENCES.

1. A.M. Afanasev and V.G. Kohn, Fiz. tverd. tela 19, 1775 (1977).

2. V.V. Aristov, V.I. Polovinkina, A.M. Afanasev and V.G. Kohn, Acta Cryst. A36, 1002 (1980).

3. V.V. Aristov, V.G. Kohn and V.I. Polovinkina, phys. stat. sol. (a) 62, 431 (1980).

4. V.V. Aristov, V.G. Kohn, V.I. Polovinkina and A.A. Snigirev, phys. stat. sol. (a) 72, 483 (1982).

5. T. Tuomi, M. Tilli, V. Kelhä and J.D. Stephenson, phys. stat. sol. (a) 50, 427 (1978).

6. A. Guinier and J. Tennevin, Acta Cryst. 2, 133 (1949).

7. N. Kato and A.R. Lang, Acta Cryst. 12, 787 (1959).

8. V.V. Aristov, T. Ichikawa, S. Kikuta and V.I. Polovinkina, Japan. J. Appl. Phys. 20, 1947 (1981).

9. V.L. Indenbom, I.S. Slobodetsky and K.G. Truni, Zh. Eksp. Teor. Fiz. 66, 1110 (1974).

10. E.V. Suvorov and V.I. Polovinkina, Pis'ma Zh. Eksp. Teor. Fiz. 20, 328 (1974).

11. V.L. Indenbom, E.V. Suvorov and I.S. Slobodetsky, Zh. Eksp. Teor. Fiz. 71, 359 (1976).

12. V.V. Aristov, A.M. Afanasev, V.G. Kohn, V.I. Polovinkina and A.A. Snigirev, submitted to Acta Cryst.

FIGURE CAPTIONS

Figure 1. : Sketch of the experimental setup.

Figure 2. : Topograph of the symmetric (111) reflection from a wedge shaped Si single crystal. $\lambda = 1.2$ A. $L_1 = L_2 = 0.38$ m.

Figure 3. : Scheme of the beam splitting in a two-crystal LL-interferometer.

Figure 4. : Diagram of the interference structure of the successive Laue diffraction image of X-ray spherical waves in two crystals (a) $L = 0$, (b) $L >> 0$.

Figure 5. : Topographs of a two-crystal interferometer for the Si (220) reflection at $L_1 = L_2 = 0.1$ m, $\lambda = 1.0$ A. (a) twice diffracted beam E_{hh}, (b) beam E_{h0}, (c) beam E_{0h}.

Figure 6. : Topographs of a two-crystal interferometer for the Si (220) reflection at $L_1 = L_2 = 0.4$ m, $\lambda = 1.0$ A. (a) beam E_{h0}, (b) beam E_{0h}.

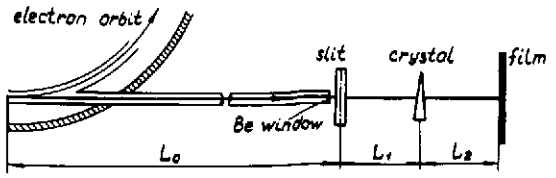

Fig. 1

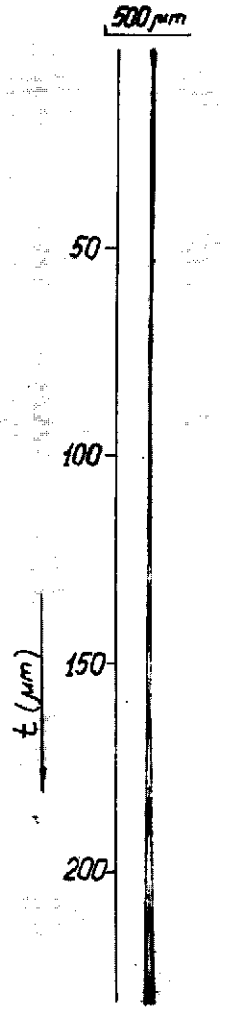

Fig. 2

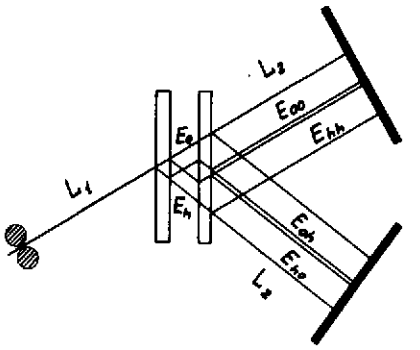

Fig. 3

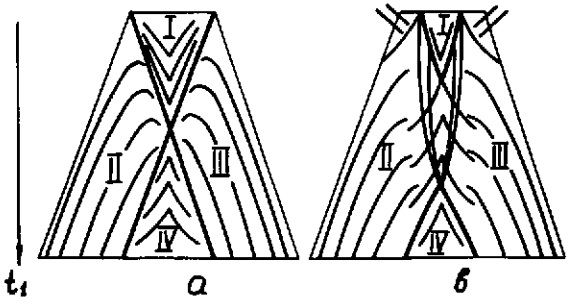

Fig. 4

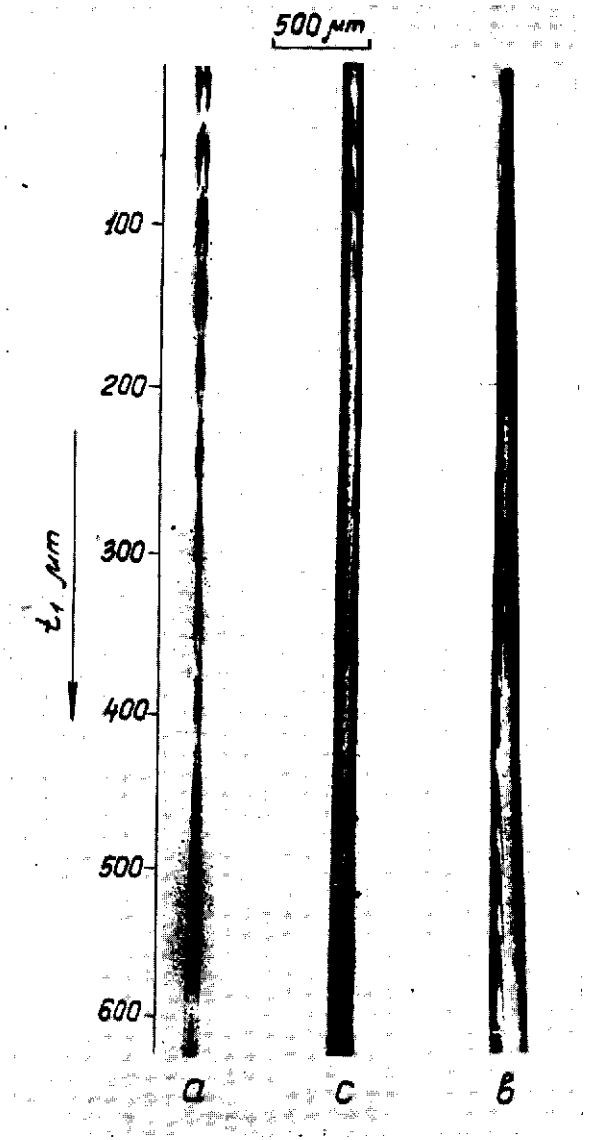
500 μm
100
200
300
400
500
600
t_1 μm
a
c
в

Fig. 5

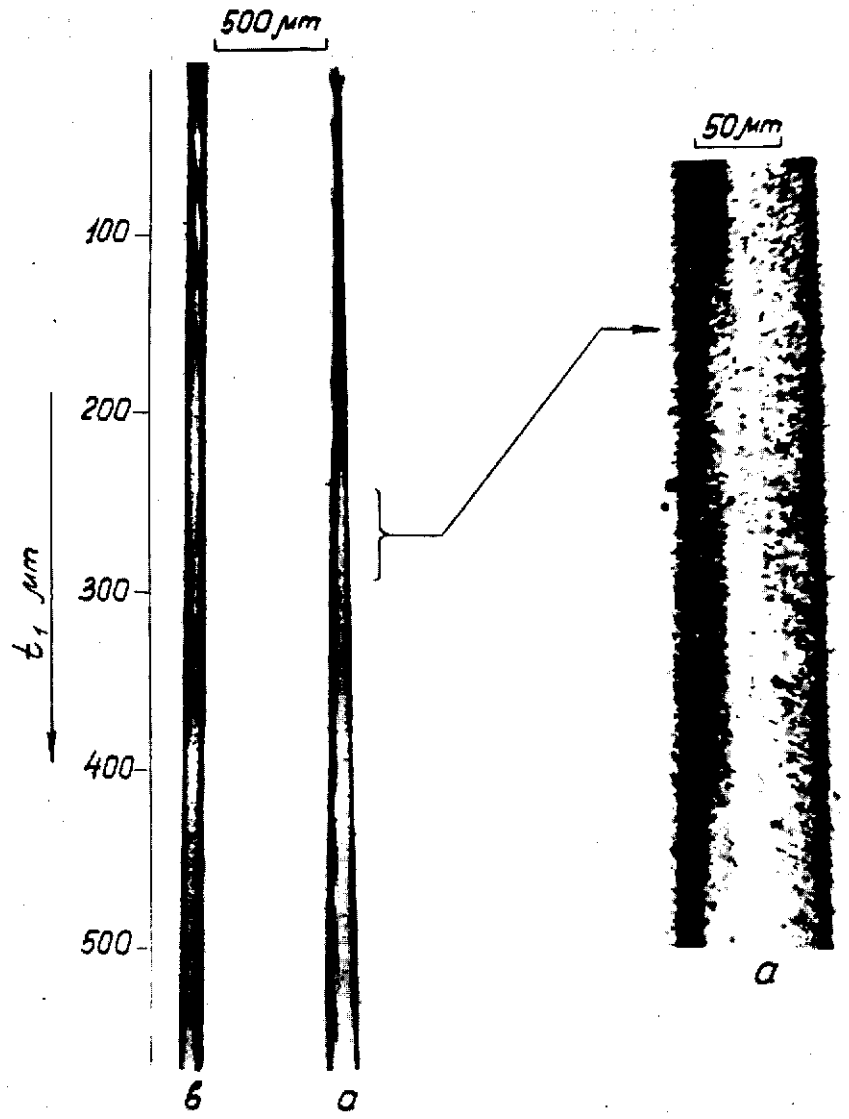
500 μm
50 μm
100
200
300
400
500
t_1 μm
в
a
a

Fig. 6